

Spatial Dependence of the Sheath Power Transmission Factor in DIII-D*

A. H. Futch, G. F. Matthews[†], D. Buchenauer[‡], D. N. Hill, and G. D. Porter

Lawrence Livermore National Laboratory
Livermore, CA, 94550

Abstract. The spatial dependence of the power transmission factor, d , associated with an ion-electron pair passing through the sheath at the DIII-D divertor plate has been determined by sweeping the edge plasma across Langmuir probe detectors. Our results show that d decreases from the classically expected value of eight near the low density edge of the scrape-off-layer plasma to values less than unity at the peak of the profile.

MASTER

*This work was performed under the auspices of the U. S. Department of Energy by the Lawrence Livermore National Laboratory under Contract W-7405-ENG-48.

[†]Culham Laboratory, Abingdon, Oxon, United Kingdom

[‡]Sandia National Laboratories, Livermore, CA.

EP

1. Introduction

In this paper we re-examine previous measurements of δ where values in the range of 2 to 3 were reported (Ref. 1). The theoretical value of δ expected from Stangeby's formula (Ref. 2)

$$\delta = \frac{2T_i}{T_e} + \frac{2}{1-\gamma_e} - 0.5 \ell n \left[2\pi \frac{m_e}{m_i} \left(1 + \frac{T_i}{T_e} \right) (1-\gamma_e)^{-2} \right] , \quad (1)$$

is approximately eight if the secondary electron emission coefficient, γ_e , is zero. Inclusion of current flow or secondary electron emission increases the value of δ , and therefore, the discrepancy between theory and the reported measurements becomes larger. The authors of Ref. 1 suggest that the anomalously low measured values of δ in DIII-D results from an effective ion collecting area which is much larger than the projected geometric area. This explanation was suggested by experiments on DITE (Ref. 3), where measurements using a tilting array of flush-mounted Langmuir probes showed the effective ion collection area to be much larger than the projected geometric area if the angle between the divertor tiles and the magnetic field is less than 10° .

To determine δ , we equate the expression for the power flow to the DIII-D divertor tiles as calculated from the Langmuir probe data (Ref. 4) to IR camera measurements of the heat flux (Ref. 5), P_{IR} , deposited on divertor tiles. Since the power flow as calculated from a Langmuir probe is $P_{LP} = \delta I_{sat} T_e \sin \theta / A_\perp$, where $\theta = \theta_D + \theta_t$ is the angle between the floor tiles and the magnetic field direction, and θ_t

is the deviation from the horizontal plane of any particular floor tile and $\theta_B = B_n/B_\phi$, the expression for δ becomes

$$\delta = \frac{P_{IR} A_{\perp}}{I_{sat} T_e \sin \theta} \quad (2)$$

In Eq. (2), I_{sat} is the measured ion saturation current, and A_{\perp} is the projected area of the probe perpendicular to the plasma flow.

In our re-examination of the DIII-D data, we find a large time dependence of δ during a shot. This observation eliminates the suggestion that the anomalous low value of δ results from an effective area much larger than the geometric area since the field angle does not vary significantly during the shot. We relate the large changes in δ during a shot to the spatial dependence of δ as the edge plasma profile is swept across the Langmuir probes, and suggest that the anomalously low values of δ results from localized gas densities produced by recycling of the divertor current.

2. Experiment

The experiment arrangement shown in Fig. 1 is the same as that discussed in Ref. 1. Although 21 Langmuir probes have now been installed across the divertor floor to provide profile data without the necessity of sweeping, the data analyzed here is limited to the previous configuration with Langmuir probes installed in only two locations. The design of the Langmuir probes are similar to those used on JET and are domed to produce a projected area, A_{\perp} , which is insensitive to the field angle over the range of field angles typical of the DIII-D divertor ($0 \rightarrow 5^{\circ}$). The IRTV camera system installed near the top of the DIII-D vacuum tank views the divertor floor and Langmuir probes as shown in Fig. 1. Results presented here are from the two probes located near the outer strike point at major radii of 1.707 m and 1.735 m. In some of the data the strike point was swept over the probes several times during the discharge. In other shots the strike point varied unintentionally early in time during the discharge and more slowly as equilibrium was approached. The angle of the magnetic field with respect to the divertor tile is approximately constant during an individual shot even though sweeping occurs, since it is the radial and not the vertical field which is altered during a sweep. The data has been corrected for the difference in $\sin \theta$ between the two probe locations as well as for the difference between shots. For example, θ had average values of 3.8° at $R = 1.707$ m and 4.65° at $R = 1.735$ m during the time period of 1 to 2.4 s for the discharge of Shot 66837. In analyzing the IRTV data, we also correct for the fact that the tile on which the IRTV data was recorded is tilted at an angle of 0.3° such that the deposited power is increased.

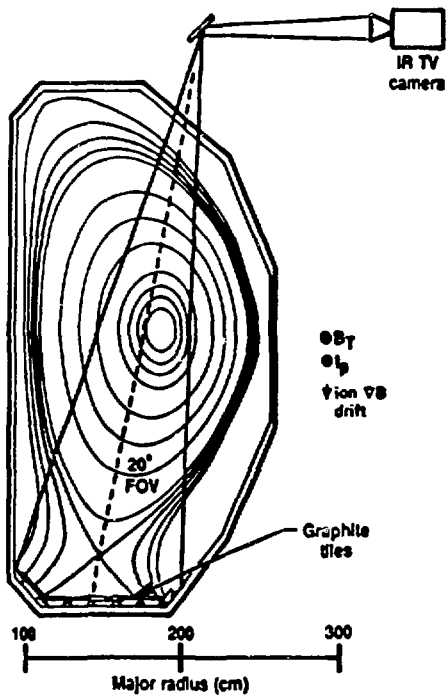


Fig. 1. Schematic view of DIII-D showing the divertor floor tiles containing the Langmuir probes.

3. Experimental Results

Plasma parameters and associated magnetic field parameters are shown in Fig. 2 as a function of time for Shot 66837 which is a typical non-swept shot that we have analyzed. The various parameters plotted in this figure are defined in the captions for the figure. Figure 3 shows a time-dependent plot of δ for the Langmuir probe at 1.735 m. Early in the shot (0.5 to 1.3 s) δ is approximately 6, but then decreases to values below 2 as the strike point approaches the detector (see curve *f* of Fig. 2 where the distance between the detector and the strike point is plotted). At approximately 2.2 s, the neutral beams turn on, the strike point begins to move away from the Langmuir probe, and δ begins to increase back to the 8 to 10 range. Values above 8 appear to be associated with either the presence of enhanced visible Bremsstrahlung (curve *g* of Fig. 2) or the presence of ELMs. Very large values of δ during ELM activity probably result from radiative power being detected by the IRTV camera instead of power lost by an ion-electron pair passing through the sheath potential. We have therefore limited our discussion in the rest of this paper to non H-mode data which we believe to be not unduly influenced by radiation. We have also excluded from consideration any data points which appear to be in the private flux region since any particle flow for this region is very small and the resulting error is likely to be large.

The time dependent values of n_e and T_e are given in Fig. 4(a) and Fig. 4(b) for the Langmuir probe at 1.735 m. Figure 5(a) shows calculated values of δ versus $n_e \sqrt{T_e}$ for the non H-mode data of Shot 66837 at the radial location of 1.735 m. Figure 5(b) shows the corresponding curve for the detector at 1.707 m. We have chosen to plot δ versus $n_e \sqrt{T_e}$ since this quantity should be proportional to the particle flux striking

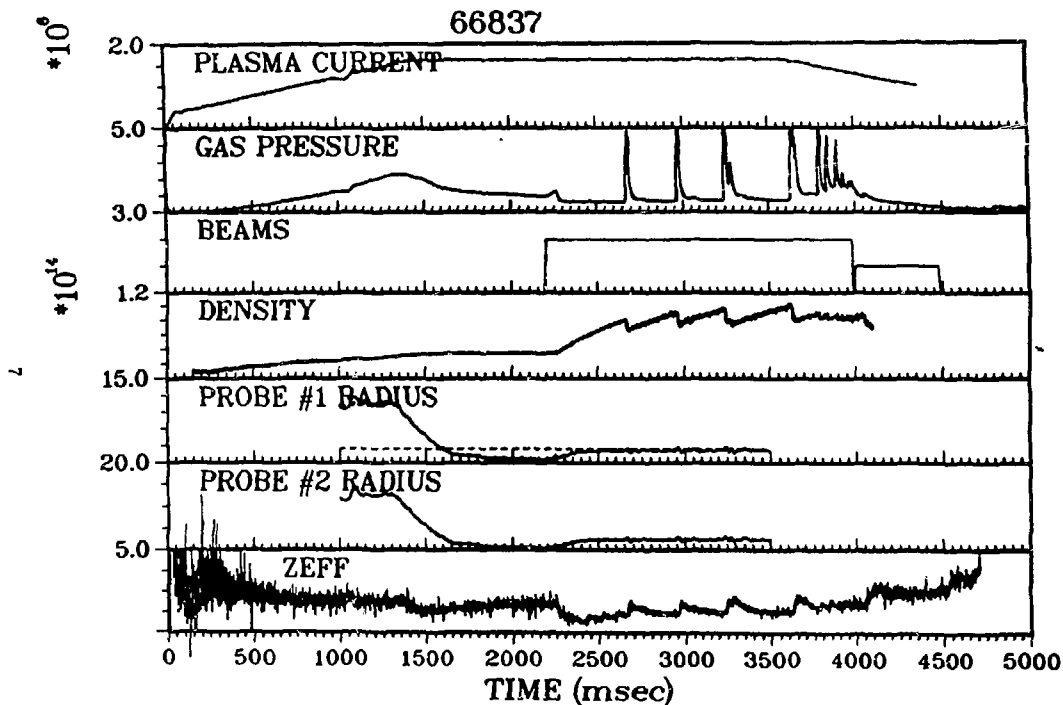


Fig. 2. Plasma parameters and associated magnetic field parameters for Shot 66837. Curves a through g are the plasma current in amperes, relative neutral gas pressure, number of neutral beams, plasma density in cm^{-3} , Langmuir probe #1 radius relative to the outer strike point in cm, Langmuir #2 radius relative to the outer strike point in cm, effective z for the plasma.

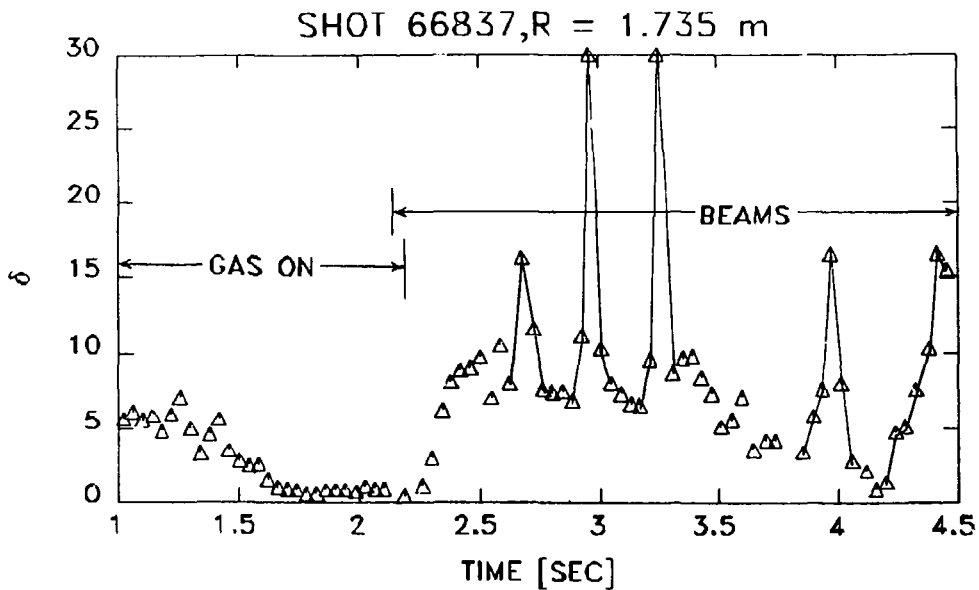


Fig. 3. Time dependent plot of the sheath power transmission factor, δ for Shot 66837 at $R = 1.735$ m.

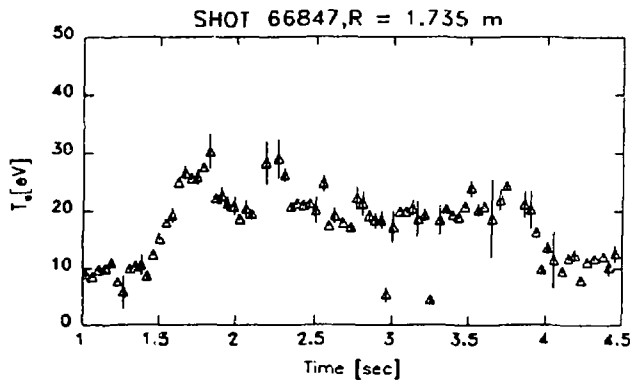
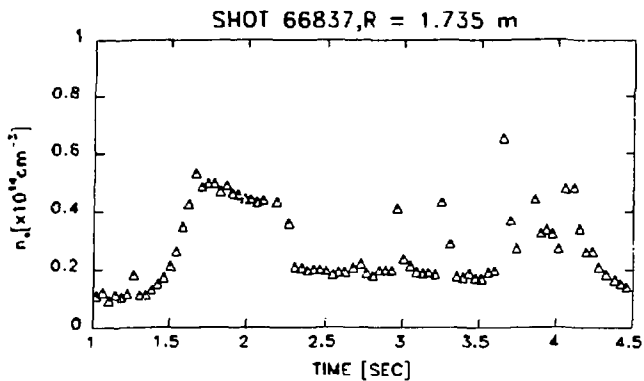


Fig. 4. Time dependent plots of the electron density (a) and the electron temperature (b) for Shot 66837.

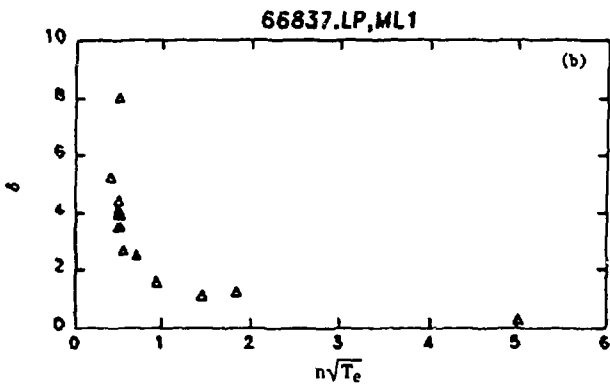
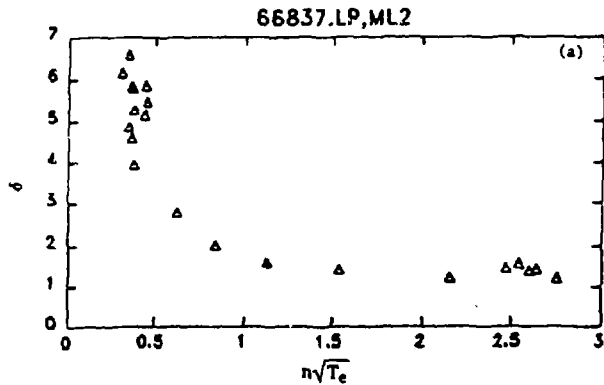


Fig. 5. The power transmission factor, δ , versus $n\sqrt{T_e}$ for Shot 66837 at (a) $R = 1.735$ m and at (b) $R = 1.707$ m.

the detector, and based on DEGAS modelling, we have speculated that this quantity is proportional to the local gas density. Both of these curves show δ to be close to the expected value of eight near the edge of the scrape-off-layer profile where $n\sqrt{T_e}$ is small and decreasing to values in the range of two or lower at the peak of the profile. We find this behavior to be consistent for all the shots we have analyzed. Figures 6 and 7 show similar results for two additional shots; these are Shots 66835 and 66840, respectively. The results for all of these shots are plotted on the same graph in Fig. 8.

Shot 66796 is one of the shots where the strike points are swept across the two Langmuir probes three times during the shot. This is also the shot which was analyzed in Ref. 1. Figure 9 shows the time dependence of plasma parameters and associated magnetic field parameters. These parameters are defined in the captions for this shot. The value of δ as a function of time is given in Fig. 10.

In Fig. 11, δ is plotted versus the parameter $n_e\sqrt{T_e}$ for Langmuir probes located at both radial locations (1.707 m and 1.735 m). The plasma for this shot is produced by the injection of deuterium beams onto a hydrogen plasma, i.e., H_2 gas is used to initiate the discharge. Although the D^+ beams are ramped up to 4.5 MW, the discharge remains in the L-mode for the entire shot duration. The uncertainty in δ observed for Shot 66796 seems somewhat greater than for the non-swept shots. In addition, for $n_e\sqrt{T_e}$ in the range from 1×10^{14} to 3×10^{14} , δ is also somewhat higher. This observation is probably best illustrated in the composite plot of Fig. 12. The explanation for the increased noise and somewhat higher values of δ could be related to the fact that neutral beams up to 4.5 MW are present and significant radiative bursts are indicated by the bolometer. The spread detector also shows a high level of carbon present at this time.

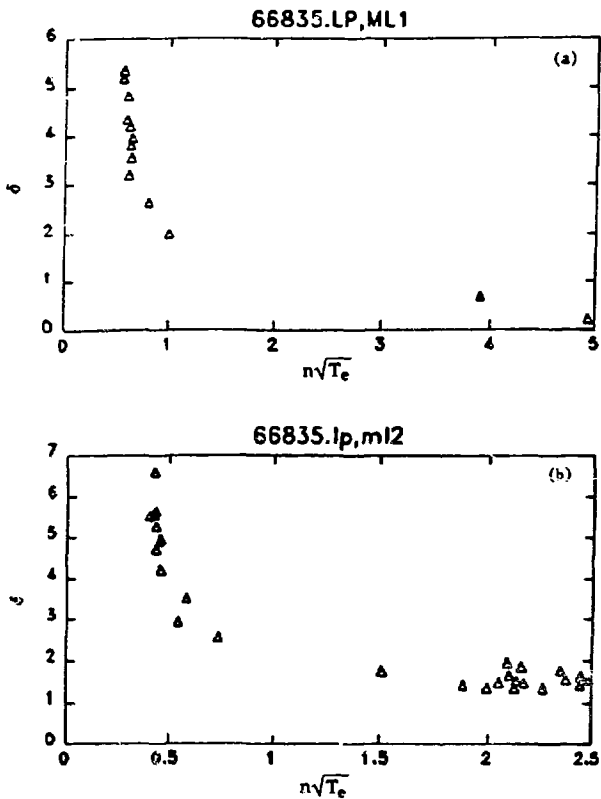


Fig. 6. The power transmission factor, η , versus $n\sqrt{T_e}$ for Shot 66835 at (a) $R = 1.707$ m and at (b) $R = 1.735$ m.

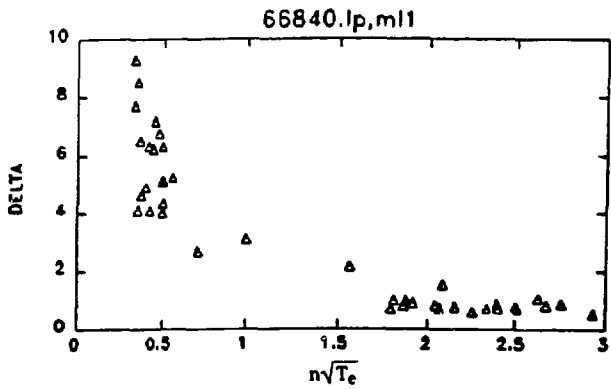


Fig. 7. The power transmission factor, δ , versus $n\sqrt{T_e}$ for Shot 66840 at $R = 1.707$ m.

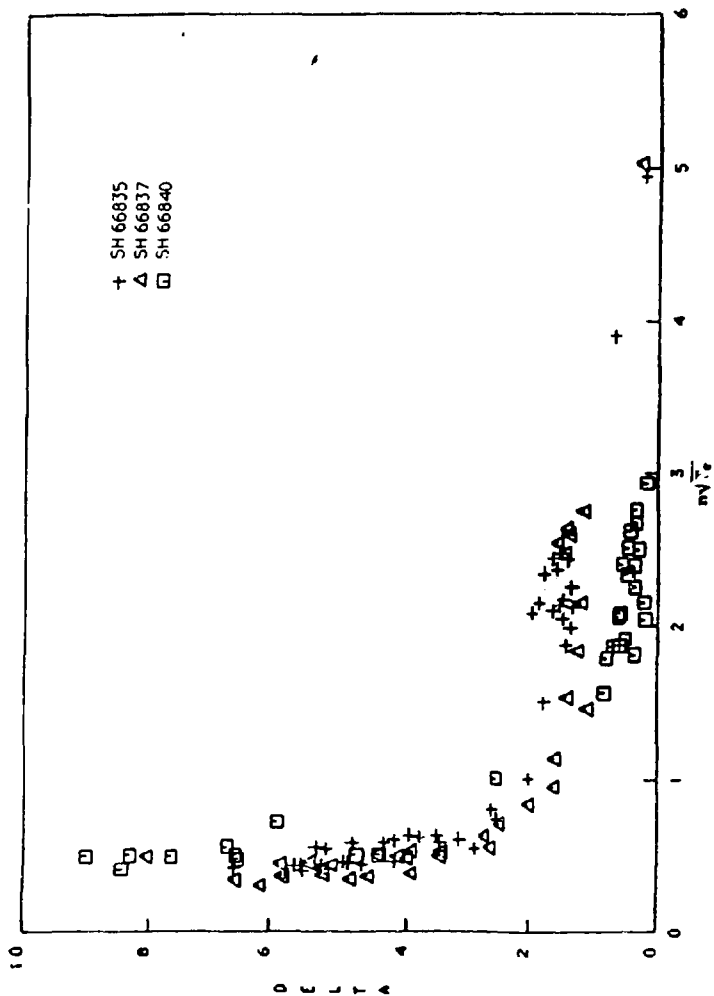


Fig. 8. Composite plot of the heat transmission factor, δ , versus $n\sqrt{x}$ for Shots 66835, 66837, and 66840.

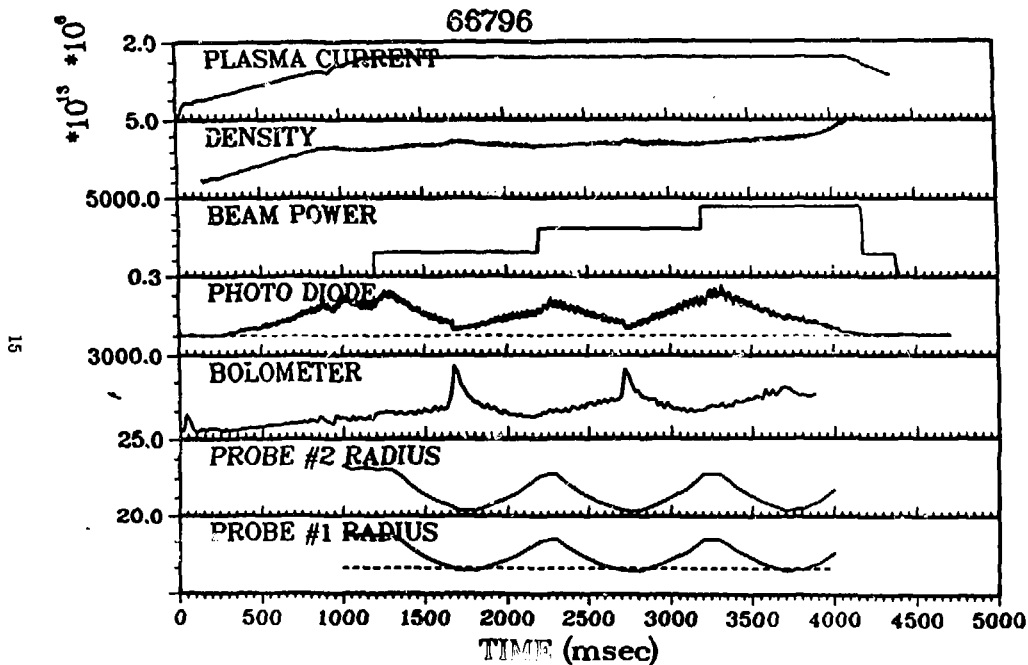


Fig. 9. Plasma parameter and associated magnetic field parameters for Shot 66796. Curves a through g are the plasma current in amperes, the plasma density in cm^{-3} , the neutral beam power in kilowatts, a photo diode signal which is proportional to $\text{H}\alpha$ emissions, a bolometer signal which measures the radiative power emitted, Langmuir probe #1 radius relative to the outer strike point, Langmuir probe #2 radius relative to the outer strike point.

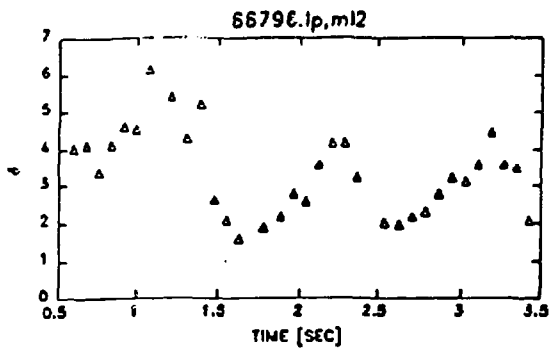


Fig. 10. Time dependent plot of the sheath power transmission factor, δ , for Shot 66796 at $R = 1.735$ m.

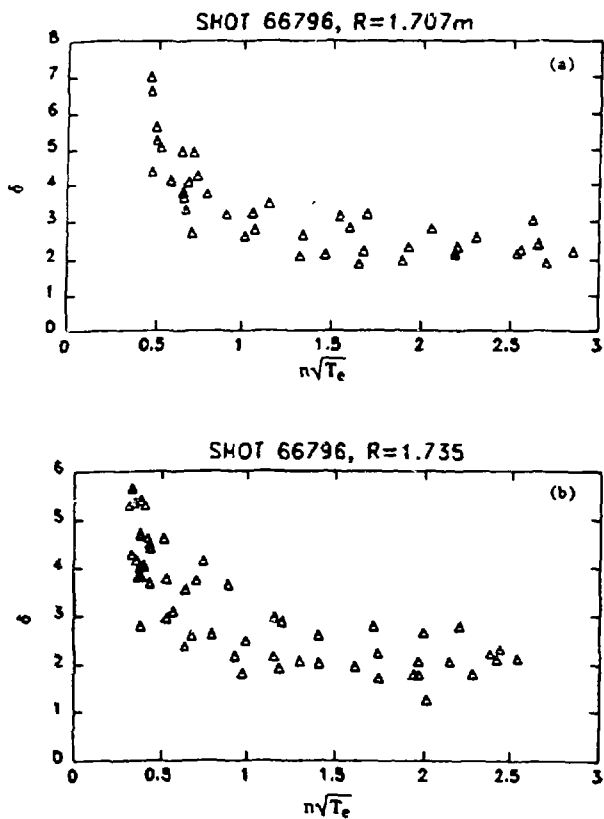


Fig. 11. The power transmission factor, δ , versus $n\sqrt{T_e}$ for Shot 66796 at (a) $R = 1.707$ m and at (b) $R = 1.735$ m.

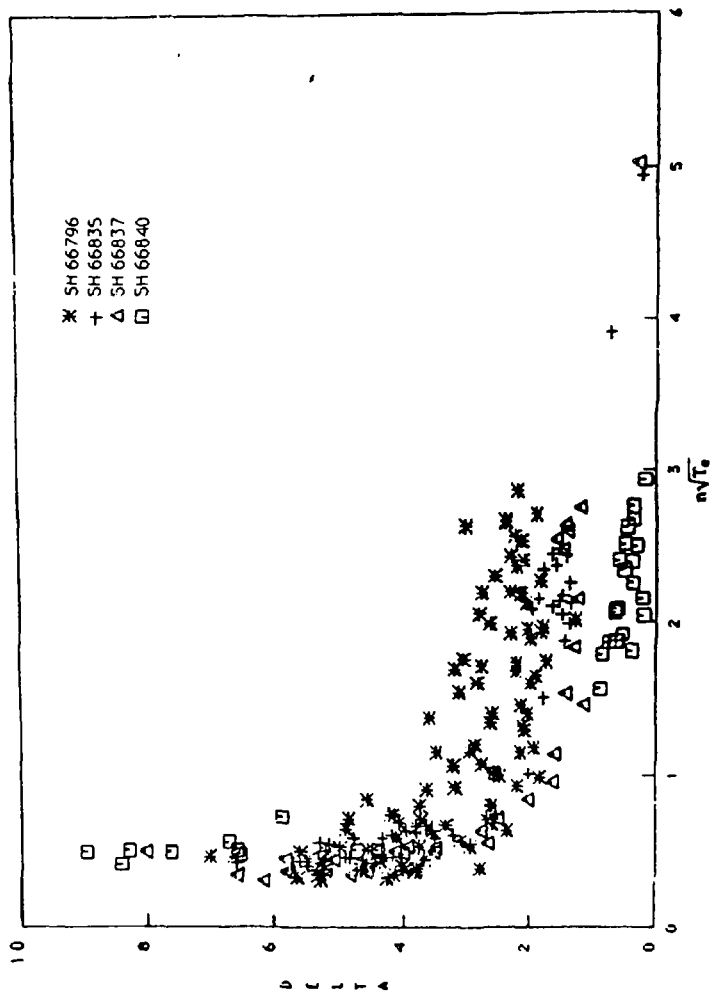


Fig. 12. Composite plot of the power transmission factor, δ , versus $n\sqrt{T_e}$ for Shots 66835, 66837, 66840, and 66796.

4. Possible Interpretation of Observed Spatial Dependence of δ

Existing theories for the electrostatic sheath potential that forms between a plasma and a wall to prevent a net flow of current solves Poisson's equation in the absence of particle sources or sinks except at the boundaries (Refs. 6-9). Using a numerical model, Cheduca studied the effect of a magnetic field on the collisionless electrostatic sheath (Ref. 10). Daybelge and Bein have also studied the collisionless electrostatic sheath in the presence of a uniform magnetic field having a small angle of incidence with respect to the surface (Ref. 11). An important feature of their results is that for negative wall potentials the scale length of the sheath in front of an absorbing wall is the ion Larmor radius, whereas for positive wall potentials this length reduces to the electron Larmor radius.

For tokamak plasmas such as DIII-D, the wall potential is negative with respect to the plasma. Therefore, according to Ref. 11, the scale length for the sheath potential perpendicular to the surface is the ion Larmor radius. Although this distance is small for the magnetic fields of DIII-D we will show that for a one-for-one recycling of plasma to neutral atoms at the divertor tiles as modeled by DEGAS, local neutral gas densities are sufficiently large, that significant atomic collisions occur within the sheath potential and the collisionless assumptions of existing theories or numerical models are not valid.

A large number of atomic collisions within the potential sheath scale length will influence the heat transmission factor δ in at least two ways. First, the potential will be different from that calculated by collisionless theory and second, ions that undergo

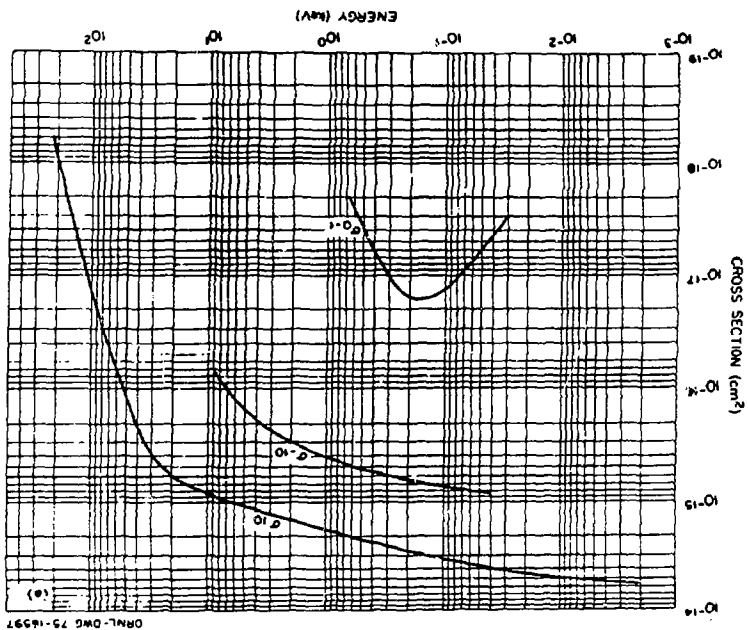
collisions within the potential sheath will no longer arrive at the wall surface with an energy of $e\phi + 2T_i^0$ where T_i^0 is the ion temperature prior to being accelerated by the sheath. From the second effect, we expect δ to decrease from the classical value of 8 to $\sim 2 \lambda_e$ for sufficiently larger neutral gas pressures. Here we have assumed Z is unity and that the ion T_i after the collision is negligible. Of course, coulomb collisions could eventually lower T_e , but the large Langmuir probe size makes spatial measurements of T_e within the sheath impossible.

Although we have no local measurements of gas pressure on the divertor tiles, the profile dependence of δ is consistent with the speculation that δ is reduced by a sufficiently large gas density near the plasma wall interface. We note that it is possible to measure a profile dependence of the floating potential and we have analyzed data from one of the shots to look for changes in the potential as the strike point moves across the Langmuir probes. We find that the floating potential decreases as the edge profile is swept across the Langmuir probe and will discuss this result later in this section.

We now attempt to justify our claim that a collisionless potential theory is not valid for the divertor tiles in DIII-D and that a lower power transmission factor is expected for sufficiently high neutral gas pressures. Although we have no direct measurements of the local gas pressure at the strike points, DEGAS modelling of gas densities in several locations along the DIII-D vacuum walls have been consistent with measurements of gas densities at these locations (factor of 2 agreement). For our estimate of the gas pressure under the strike point we use the DEGAS results from SEP2790 which is a run for a standard L-mode discharge. The atomic neutral density number under the peak of the outer strike point was 2.7×10^{15} atoms/cm³.

From the measured charge exchange σ_{cx} and elastic scatterings σ , cross-sections given in Fig. 13(a) and (b), respectively, we obtain approximate values of 5×10^{-15} cm² and 1×10^{-14} cm² for a 10 eV H⁺ ion. These cross-sections are observed to be slowly

Fig. 13. Charge exchange (a) and elastic scattering cross section (b) from Ref. 12. (Sheet 1 of 2)



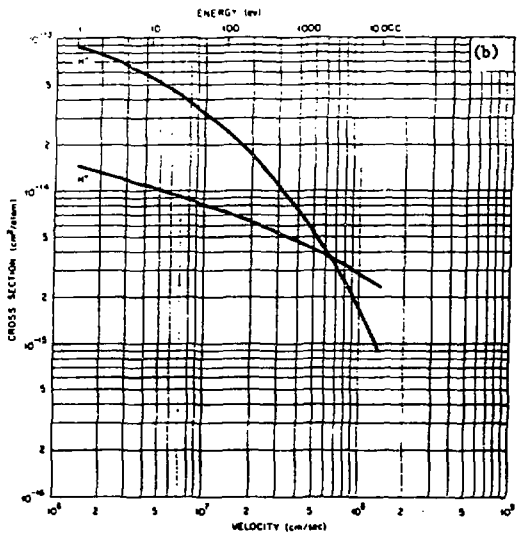


Fig. 13. Charge exchange (a) and elastic scattering cross section (b) from Ref. 12. (Sheet 2 of 2)

varying at this energy. A neutral D^0 atom will penetrate a distance $\lambda = (n_e \sigma_{cs})^{-1} = 5.7$ cm before being converted into an ion by a charge exchange collision. Therefore the neutral density is essentially constant over the potential scale length. Electron ionization will not significantly reduce this distance since the electron ionization cross-section is smaller than the resonance charge exchange cross-section. Calculating the mean free path for an ion to lose energy by either charge exchange or elastic scattering as $(n_e \cdot s)^{-1}$, we find the mean free path to be 0.07 cm and 0.04 cm, respectively. Either one of these collisions will reduce the energy the ion gained in falling through the potential sheaths and lead to a reduction in δ . Including both of these processes, we obtain a combined mean free path λ_t of

$$\frac{1}{\lambda_t} = \frac{1}{\lambda_{cs}} + \frac{1}{\lambda_s} = 40 \text{ cm}^{-1} , \quad (3)$$

or $\lambda_t = 2.5 \times 10^{-2}$ cm. The ion Larmor radius is

$$\rho = \frac{2 \times 10^2}{B} \sqrt{E} = 3.2 \times 10^{-2} \text{ cm} , \quad (4)$$

for an ion energy of 10 eV and a magnetic field of 2 T. An ion moving along the field line will be in the potential sheath region for a distance of $\rho/\sin \theta \approx 0.5$ cm for $\theta = 4$ degrees which is a typical value of θ at the divertor strike point. Although a finite temperature perpendicular to the magnetic field can shorten this distance, we conclude that the mean free path for atomic collision is less than the scale length for the potential sheath and therefore an ion passing through the potential sheath has a good probability of losing energy as a result of collisions before reaching the wall surface. This energy loss will result in a smaller value for the power transmission factor. We have also pointed out that the inclusion of collisions in the sheath theory

could also change the magnitude of the potential itself which would lead in turn to a lower transmission factor if the sheath potential is smaller.

For a non-magnetic plasma, the sheath potential can be obtained from the exponential dependence of the I-V characteristic for the Langmuir probe above the floating potential, V_f . In a strongly magnetized plasma, the I-V characteristic is observed to be non-exponential for voltages above V_f . In addition plasma fluctuations further distorts the I-V characteristic especially above the floating potential making probe measurements of the sheath potential unreliable. However, we have obtained measurements of the floating potential and also observed a correlation between the power transmission factor, δ , and the floating potential.

Figure 14 shows the measured floating potential, V_f , versus $n\sqrt{T_e}$ for shot 66796 at $R = 1.735$ m which is the swept shot discussed earlier. The time dependence of both the floating potential and δ is exhibited in Fig. 15, and in Fig. 16, the floating potential is plotted versus δ . The straight line in the figure is a least squares fit to the experimental data. This observed correlation is inconsistent with existing models for the power transmission factor (Ref. 6-11, 13) where δ is independent of the floating potential. Here again, a possible explanation for this paradox is that both V_f and δ are functions of another parameter which we suggest is the local neutral gas pressure. The large decrease in δ as the profile is swept across the detector requires both a decrease in the sheath potential as well as a decrease in the kinetic energy of the ions and electrons prior to the potential sheath drop. This is additional evidence that the local gas pressure has an effect on the sheath potential as well as the measured effect on the floating potential.

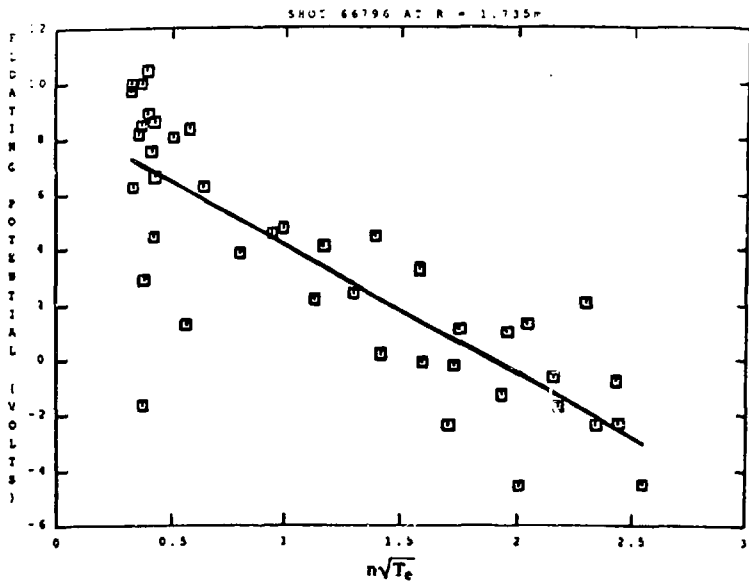


Fig. 14. The dependence of the floating potential, V_f , as a function of $n\sqrt{T_e}$ for Shot 66796 at $R = 1.735$ m, the straight line is a least square fit of the equation $V_f = a(0) + a(1)n\sqrt{T_e}$ through the data points where $a(0) = 8.75$ and $a(1) = -4.63$.

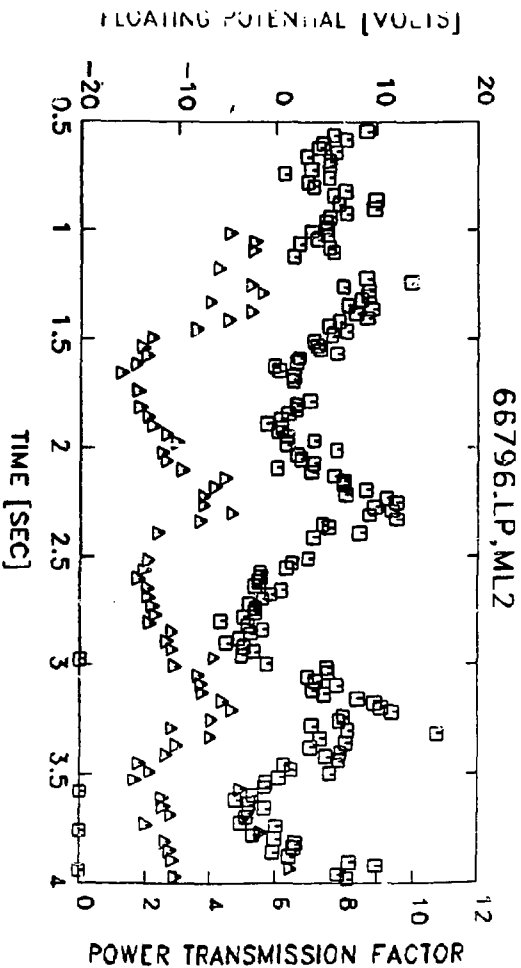


Fig. 15. The time dependence of the floating potential and the power transmission factor for Shot 66796 at $R = 1.735$ m.

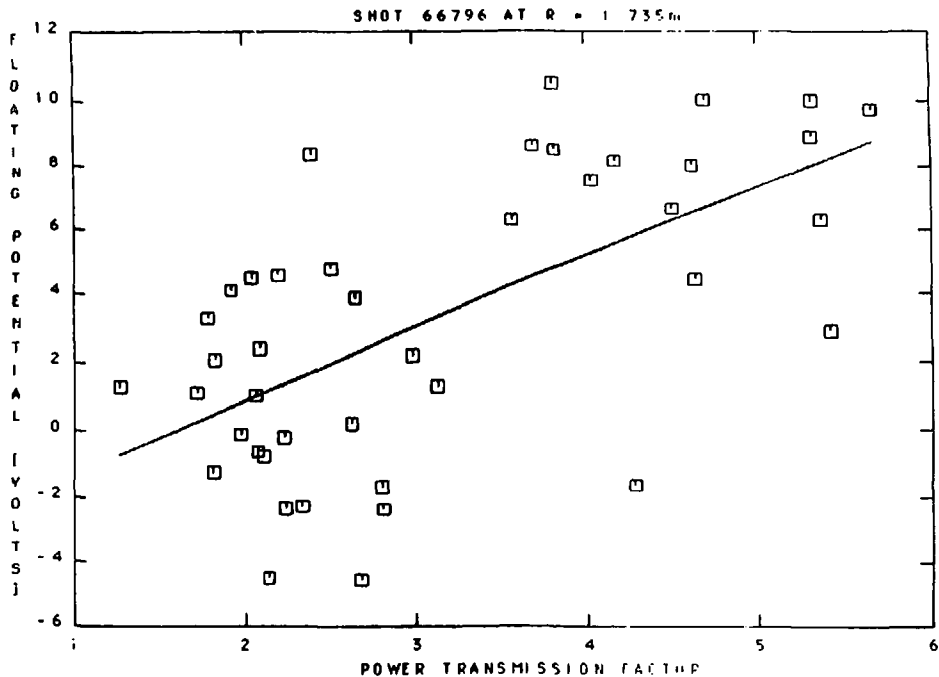


Fig. 16. The floating potential versus the power transmission factor for Shot 66796 at $R = 1.735$ m. The straight line is a least squares fit of the equation $V_f = a(0) + a(1)\delta$ through the data points where $a(0) = -3.46$ and $a(1) = 2.17$.

References

1. G.F. Matthews, D. Buchenauer, D.N. Hill, and M.A. Mahdavi, "The Sheath Power Transmission Factor in DIII-D," General Atomics Report GA-A20337, October 1990 submitted to Plasma Physics and Controlled Fusion.
2. P.C. Stangeby in "Physics of Plasma-Wall Interactions in Controlled Fusion," Plenum Press, New York, 1986 (D.E. Post and R. Behrisch, eds.) pp. 41-97.
3. G.F. Matthews, G.M. McCracken, P.C. Stangeby, "Plasma Physics and Controlled Fusion," to be published.
4. D. Buchenauer, W.L. Hsu, J.P. Smith, D.N. Hill, Rev. Sci. Instru. **61**, 2873, (1990).
5. D.N. Hill, R. Ellis, W. Ferguson, D.E. Perkins, T. Petrie, C. Boxi, Rev. Sci. Instru. **59**, 1879 (1988).
6. G.D. Hobbs and J.A. Wesson, Plasma Physics **9**, 85 (1967).
7. G.D. Hobbs and J.A. Wesson, Culham Laboratory, Report CLM-R61 (1966).
8. G.D. Porter, Nucl. Fusion **22**, 1279 (1982).
9. L.S. Hall, Nucl. Fusion **17**, 681 (1977).
10. R. Chodura, Phys. Fluids **25**, 1628 (1982).
11. V. Daybelge and B. Bein, Phys. Fluids **24**, 1190 (1981).
12. C.F. Barnett, Oak Ridge National Laboratory Report ORNL-3113 (revised) (1961).
13. P.C. Stangeby and G.M. McCracken, Nucl. Fusion **30**, 1225 (1990).